

# Nickel–Aluminum Intermetallic Compounds as Highly Selective and Stable Catalysts for the Hydrogenation of Naphthalene to Tetralin

Xiao Chen, Yue Ma, Lei Wang, Zonghan Yang, Shaohua Jin, Liangliang Zhang, and Changhai Liang\*<sup>[a]</sup>

Selective hydrogenation of naphthalene to tetralin was conducted by using Ni–Al intermetallic compounds (IMCs) prepared by a chemical synthetic route. Ni–Al IMC catalysts achieved a lasting high conversion with 100% selectivity up to 125 h. During the synthesis process, the Ni–Al IMCs underwent the following phase transformation as a function of the content of the Al source ( $\text{LiAlH}_4$ ):  $\text{Ni}(\text{cubic}) \rightarrow \text{Ni}_3\text{Al}(\text{tetragonal}) \rightarrow \text{NiAl}(\text{cubic}) \rightarrow \text{Ni}_2\text{Al}_3(\text{hexagonal})$ . In the selective hydrogenation of naphthalene, the catalytic activity of NiAl was much higher

than that of metallic Ni and other Ni–Al IMCs ( $\text{Ni}_3\text{Al}$  and  $\text{Ni}_2\text{Al}_3$ ). The results can be understood by a combination of site isolation and alteration of the electronic structure by chemical bonding. Ni atoms are scattered and spatially isolated by Al atoms, which in turn resists carbon deposition. The findings provide a useful approach to tailor the catalytic properties of transition metals by formation of IMCs, which could be applicable in heterogeneous catalysis.

## Introduction

Tetralin, a useful high-boiling-point solvent, has been widely used in paints, coatings, inks, pharmaceuticals, and paper, and it has additionally been used as a hydrogen donor.<sup>[1]</sup> It can be synthesized simply through the semihydrogenation of naphthalene.<sup>[2,3]</sup> The heterogeneous hydrogenation of naphthalene is not only a useful model reaction that can be used to gauge the activity of metal catalysts, but it is also of industrial importance in upgrading coal liquids and diesel fuels.<sup>[4]</sup> This process not only improves the stability of fuels, but it also reduces emissions of harmful solid particles. Traditionally, transition-metal sulfide catalysts have low activity and need high operation temperatures owing to thermodynamic limitations of the hydrogenation of aromatics.<sup>[5]</sup> In addition, noble-metals catalysts exhibit high activity, but they are always limited in their application because of their high price and poisoning of their active sites by sulfur, nitrogen, and carbon atoms.<sup>[6]</sup> Therefore, the development of highly active catalysts with long-term stability for the selective hydrogenation of naphthalene is of great importance.<sup>[7]</sup>

Intermetallic compounds (IMCs), such as transition-metal aluminides, are between metal alloys and ionic compounds; they exhibit unique physical and chemical properties (high melting point, low density, and high corrosion resistance).<sup>[8,9]</sup> Owing to charge transfer and hybridization between the Al s and p

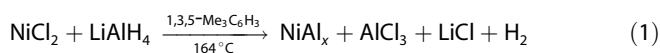
states and the transition-metal d states, transition-metal aluminides with a special geometry and electronic structure have potential applications in catalysis.<sup>[10–14]</sup> Ganem and Osby reviewed the applicability of metal aluminide catalysts in some typical organic reactions, which laid the foundation for the rational design of efficient aluminide compounds as new catalytic materials.<sup>[11]</sup> Recently, on the basis of the theory of site isolation and alteration of the electronic structure by chemical bonding, Armbrüster et al. successfully synthesized the noble-metal-free and environmentally benign IMCs  $\text{Al}_{13}\text{Fe}_4$  and  $\text{Al}_{13}\text{Co}_4$ , which were identified as potent and low-costing replacements for Pd-based hydrogenation catalysts in the partial hydrogenation of acetylene.<sup>[12,13]</sup> Subsequently, Piccolo further confirmed that  $\text{Al}_{13}\text{Fe}_4$  was a selective hydrogenation catalyst for butadiene at room temperature under well-defined ultra-high vacuum conditions.<sup>[14]</sup> Unfortunately, preparation methods for aluminides including the use of high-energy solids and interface reactions inherited from the ceramic industry result in big particle sizes and low surface areas. The controlled synthesis of a high surface area or well-dispersed metal aluminides still remains an important challenge for catalytic applications. Herein, we report the synthesis of nanocrystalline nickel aluminides that exhibit excellent selectivity and long-term stability in the selective hydrogenation of naphthalene.

[a] Dr. X. Chen, Y. Ma, L. Wang, Z. Yang, S. Jin, L. Zhang, Prof. C. Liang  
Laboratory of Advanced Materials and Catalytic Engineering  
School of Chemical Engineering  
Dalian University of Technology  
Dalian 116024 (P.R. China)  
E-mail: changhai@dlut.edu.cn

Supporting Information for this article is available on the WWW under <http://dx.doi.org/10.1002/cctc.201402957>.

## Results and Discussion

The Ni–Al phase diagram contains five IMCs:  $\text{Ni}_3\text{Al}$ ,  $\text{Ni}_5\text{Al}_3$ , NiAl,  $\text{Ni}_2\text{Al}_3$ , and  $\text{NiAl}_3$ . Ideally, the specific intermetallic phase produced by reaction of  $\text{NiCl}_2$  with  $\text{LiAlH}_4$  would be controlled by stoichiometry, as proposed in Equation (1).<sup>[15,16]</sup>



In this work, the molar ratio of  $\text{NiCl}_2$  and  $\text{LiAlH}_4$  was controlled at 4:3, 4:5, 4:7, and 4:9. The microstructures of the as-prepared samples were determined by X-ray diffraction (XRD; see Figure S1, Supporting Information).  $\text{NiCl}_2$ , metal Al, and produced  $\text{LiCl}\cdot\text{H}_2\text{O}$  were detected, but metallic Ni and Ni–Al IMCs were missing. It is presumed that the intermetallic phases did not directly form during the solvent step and that further annealing was required to transform the as-precipitated powders yielded in the solvent step to drive the reactions to completion.

The XRD patterns of the samples annealed at  $650^\circ\text{C}$  under an atmosphere of Ar are shown in Figure 1a. Typical diffraction peaks at  $2\theta = 44.5$ ,  $51.8$ , and  $76.4^\circ$  can be detected in the  $\text{NiAl}_{3/4}$  sample, and these peaks correspond to cubic-phase

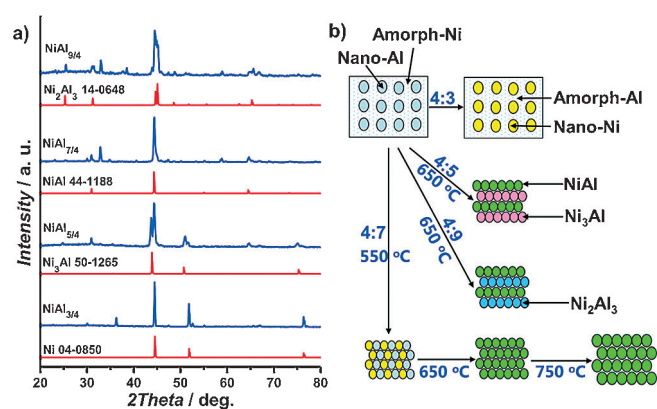


**Figure 1.** a) XRD patterns of Ni–Al IMCs with different molar ratios annealed at  $650^\circ\text{C}$ . b) Simplified schematic representation of the reaction pathways.

nickel (JCPDS No. 04-0850). At the same time, trace amounts of  $\text{NiCl}_2$  were residual, which indicates that superfluous  $\text{LiAlH}_4$  is needed to promote the formation of Ni–Al IMCs. By increasing the content of the Al source ( $\text{LiAlH}_4$ ), the diffraction peaks at  $2\theta = 43.9$ ,  $50.7$ , and  $75.3^\circ$  attributable to the (112), (004), and (220) reflections of tetragonal-phase  $\text{Ni}_3\text{Al}$  (JCPDS No. 50-1265), respectively, are observed in the XRD pattern of the  $\text{NiAl}_{5/4}$  sample. In addition, the sample shows typical diffraction peaks at  $2\theta = 44.3$ ,  $30.9$ ,  $64.5$ , and  $81.6^\circ$ , which indicates the formation of NiAl (cubic, JCPDS No. 44-1188). Upon decreasing the Ni/Al molar ratio to 4:7, the diffraction peaks of NiAl become sharper, whereas the peaks of  $\text{Ni}_3\text{Al}$  disappear. A further decrease in the Ni/Al molar ratio to 4:9 results in three new diffraction peaks at  $2\theta = 18.1$ ,  $25.3$ , and  $31.2^\circ$ , which can be assigned to hexagonal-phase  $\text{Ni}_2\text{Al}_3$  (JCPDS No. 14-0648). In addition, the LiCl byproduct sublimes after thermal treating. Mixtures of the desired intermetallic phases are obtained, whereas  $\text{NiCl}_2$  and metal Al are eliminated; this indicates that a reaction occurs between nanocrystalline Al and Ni. The formation of Ni–Al IMCs involves the following sequence as a function of the content of the Al source ( $\text{LiAlH}_4$ ): Ni(cubic)  $\rightarrow$   $\text{Ni}_3\text{Al}$ (tetragonal)  $\rightarrow$  NiAl(cubic)  $\rightarrow$   $\text{Ni}_2\text{Al}_3$ (hexagonal).

To probe the formation and phase transition of Ni–Al IMCs during the annealing process, the effect of temperature was further investigated. As shown in Figure S2, only metallic Ni and Al are formed upon annealing at  $550^\circ\text{C}$ . However, as the temperature is increased to  $650^\circ\text{C}$ , characteristic diffraction peaks at  $2\theta = 44.3$ ,  $30.9$ ,  $64.5$ , and  $81.6^\circ$  attributable to NiAl with a cubic structure are observed. If the temperature is raised to  $750^\circ\text{C}$ , the peaks for NiAl become sharper and peaks for  $\text{Al}_2\text{O}_3$  start to appear; consequently,  $650^\circ\text{C}$  is a key temperature for crystal transformation. The improved temperature promotes aggregation of the Ni–Al IMC nanoparticles with enhanced crystallinity. All the synthetic results are summarized in the simplified scheme of the reaction pathways (some intermediates and byproducts are omitted) in Figure 1b.

The composition and physicochemical properties of the as-prepared Ni–Al IMC catalysts are listed in Table 1. The actual

| Table 1. Composition and physicochemical properties of the Ni–Al IMC catalysts. |                                |                          |  |
|---|--------------------------------|--------------------------|--|
| Sample  | Crystalline phases             | Actual Ni/Al molar ratio | Surface area [ $\text{m}^2\text{g}^{-1}$ ] |
| $\text{NiAl}_{3/4}$   | Ni, $\text{NiCl}_2$            | 4:1.6                    | 25   |
| $\text{NiAl}_{5/4}$   | NiAl, $\text{Ni}_3\text{Al}$   | 4:3.1                    | 15   |
| $\text{NiAl}_{7/4}$   | NiAl                           | 4:5.7                    | 15   |
| $\text{NiAl}_{9/4}$   | NiAl, $\text{Ni}_2\text{Al}_3$ | 4:8                      | 14   |

compositions are similar to the nominal compositions. However, the actual Ni/Al ratios are bigger than the nominal value, which indicates that a small quantity of Al as the byproduct ( $\text{AlCl}_3$ ) is removed during the chemical route. In combination with analysis of the XRD patterns of the as-prepared Ni–Al IMCs, Al mostly reacts with Ni to form Ni–Al IMCs, but a small amount of Al exists as amorphous  $\text{Al}_2\text{O}_3$ . The BET surface areas of  $\text{NiAl}_{3/4}$ ,  $\text{NiAl}_{5/4}$ ,  $\text{NiAl}_{7/4}$ , and  $\text{NiAl}_{9/4}$  are 25, 15, 15, and  $14\text{ m}^2\text{g}^{-1}$ , respectively (Table 1). Because an increase in the amount of reducing agent (i.e.,  $\text{LiAlH}_4$ ) used produces a violent reaction during the formation of the Ni–Al IMCs in the route, the Ni–Al IMC particles aggregate, which leads to collapse of the pore structure and a decrease in the surface areas.<sup>[17]</sup> In addition, the  $\text{N}_2$  adsorption/desorption processes on the Ni–Al IMCs show incomplete type II isotherms with type H3 hysteresis loops, and this can be attributed to well-developed uniform mesoporous structures resulting from the stacking of sheet particles (as shown in Figure S3).

The SEM image and mappings of the  $\text{NiAl}_{7/4}$  sample and the corresponding energy-dispersive X-ray spectroscopy (EDX) spectrum are presented in Figure 2. Clearly, the  $\text{NiAl}_{7/4}$  particles have aggregated into an irregularly shaped sub-micrometer-sized microstructure with sintered, rounded 50–100 nm particles; this indicates that the temperature near or above the melting point of the Ni–Al IMCs ( $> 1200^\circ\text{C}$ ) may be reached in the exothermic reaction stage. Figure 2 depicts the EDX spectrum of the nanoparticles and gives quantitative information on their chemical composition, which confirms the existence of Ni and Al elements with a Ni/Al ratio of 1:1.36 in the

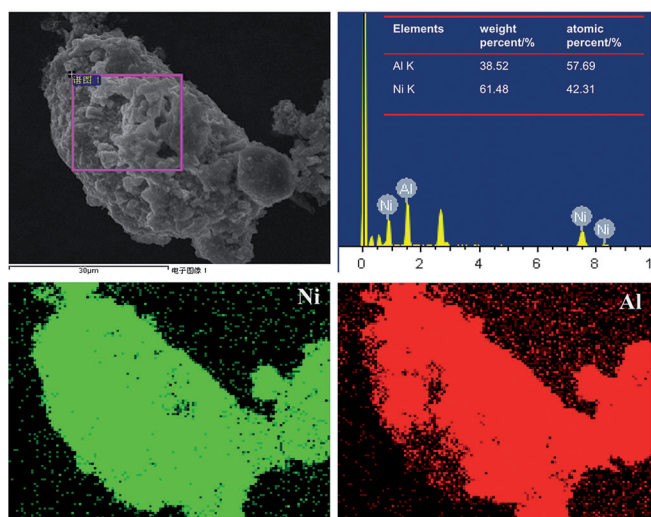


**Figure 2.** SEM image and mappings of the  $\text{NiAl}_{7/4}$  IMC catalyst and the corresponding energy-dispersive X-ray spectrum. Scale bar = 30  $\mu\text{m}$ .

sample. The result is consistent with the XRD analysis data and further confirms the formation of NiAl. Homogeneous Ni and Al distributions are found in the  $\text{NiAl}_{7/4}$  sample, as seen in the corresponding elemental maps; this indicates that the Al atoms are uniformly doped into the lattice of metallic Ni.

To investigate the structure and composition in the materials, TEM and high-resolution (HR) TEM were performed. Figure 3a shows the HRTEM image of the  $\text{NiAl}_{5/4}$  sample. The measured  $d$  value is approximately 0.2017 nm, and this can be identified as the (112) plane of the  $\text{Ni}_3\text{Al}$  phase ( $d = 0.2062$  nm). The crystalline phase was revealed as tetragonal  $\text{Ni}_3\text{Al}$  by fast Fourier transform (FFT; Figure 3a, inset). In addition, the  $d$  spacing for the (004) plane of the  $\text{Ni}_3\text{Al}$  nanoparticles was measured from such images and was found to be 0.1786 nm, which is in close agreement with the bulk value of 0.1798 nm (as shown in Figure 3b). Upon changing the Ni/Al molar ratio to 4:7, the as-prepared  $\text{NiAl}_{7/4}$  sample presents a nanosheet structure (as shown in Figure 3c), which is probably due to the formation of amorphous  $\text{Al}_2\text{O}_3$ . The HRTEM image of  $\text{NiAl}_{7/4}$  reveals its crystalline nature, with a lattice spacing of 0.2885 nm (Figure 3d), which can be indexed to the (100) crystalline plane of the cubic phase of NiAl. A further increase in the amount of Al to a Ni/Al molar ratio of 4:9 results in  $\text{NiAl}_{9/4}$  that is both uniformly dispersed and weakly aggregated (Figure 3e). The particle size is approximately 20 nm, which is close to the value obtained from Scherrer's equation. In addition, an alumina matrix also exists in the sample, which can be attributed to the excess amount of the Al source that was used in the chemical synthesis process. Figure 3f shows the HRTEM image of the  $\text{NiAl}_{9/4}$  sample. The  $d$  value measured from the image is 0.2016 nm, which is readily identified as hexagonal  $\text{Ni}_2\text{Al}_3$  [ $d = 0.2010$  nm, (102) plane]. Three types of Ni–Al IMCs ( $\text{Ni}_3\text{Al}$ , NiAl, and  $\text{Ni}_2\text{Al}_3$ ) can be obtained by changing the Ni/Al ratio in the synthetic route.

To investigate the catalytic active sites and surface-chemistry–structure relationships, the surfaces of the Ni–Al IMC catalysts were examined by XPS. Figure 4 shows the XPS spectra in

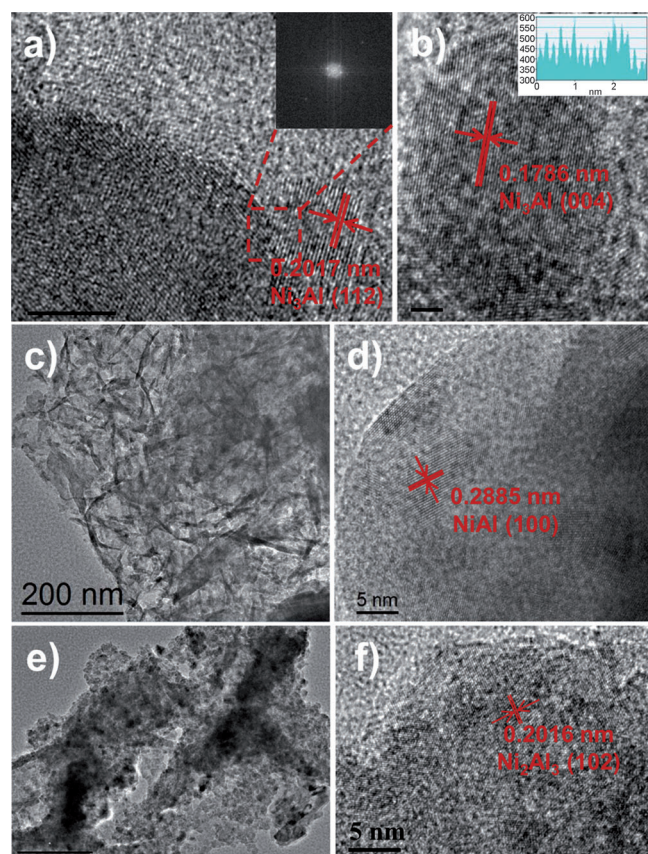


**Figure 3.** Representative low- and high-resolution TEM images of the Ni–Al IMC samples with different Ni/Al molar ratios: a, b) 4:5, c, d) 4:7, and e, f) 4:9.

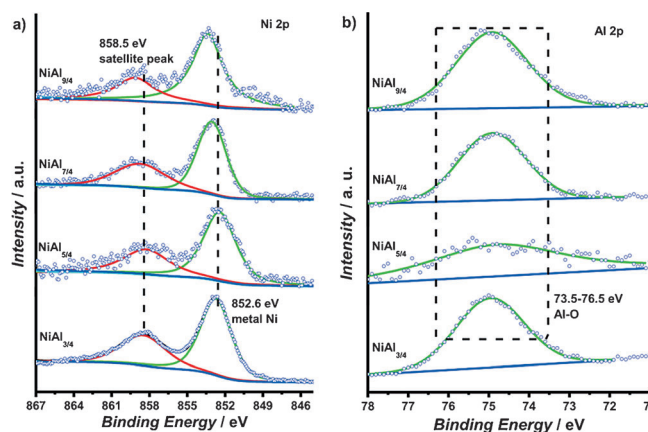


**Figure 4.** XPS of a) the Ni 2p region and b) the Al 2p region of the Ni–Al IMC samples.

the Ni 2p and Al 2p regions for the Ni–Al IMCs catalysts. The binding energy of the  $\text{Ni}2p_{3/2}$  core level for  $\text{NiAl}_{3/4}$  (Figure 4a) is 852.6 eV, which coincides well with that of pure Ni metal.<sup>[18]</sup> The chemical shifts of  $\text{NiAl}_{7/4}$  and  $\text{NiAl}_{9/4}$  in relation to metallic Ni are 0.5 and 0.8 eV, respectively. With an increase in the Al concentration in the Ni–Al IMCs, the  $\text{Ni}2p_{3/2}$  core level shifts to a positive level and the half-width decreases. In addition, the

asymmetry of the peak shape of Ni2p<sub>3/2</sub> reduces. The peak at 858.5 eV attributable to satellite peak associates with the Ni2p<sub>3/2</sub> core level of NiAl<sub>3/4</sub> and this can be attributed to the many-body effect in the photoemission process.<sup>[19]</sup> The positive shift in the satellite peak increases as the Al concentration in the Ni–Al IMCs increases. This result is similar to that of Pd in Pd–Ga IMCs.<sup>[20]</sup> Given that the transition-metal atoms are isolated by the main group elements in the IMCs, the electronic structure around the Fermi energy becomes altered.<sup>[21]</sup> Unfortunately, owing to the high concentration of Al<sub>2</sub>O<sub>3</sub> on the surface, there is an extra broad peak at 73.5–76.5 eV in the Al2p spectrum that corresponds to Al–O (as shown in Figure 4b), and this protects the samples from violent oxidation upon their exposure to air.<sup>[22]</sup>

The catalytic hydrogenation of naphthalene over Ni–Al IMCs catalysts was performed in a continuous fixed-bed reactor. The hydrogenation of naphthalene occurs in two steps (Scheme 1):



Scheme 1. Hydrogenation of naphthalene.

naphthalene is first converted into tetralin, and this is followed by the formation of decalin. As shown in Figure 5, the conversion of naphthalene over Ni–Al IMCs increases with an increase in contact time. Typically, naphthalene conversion reaches 11.3% over the NiAl<sub>7/4</sub> catalyst at a low contact time (0.44 h) and 54.6% at a high contact time (3.11 h). Among the four cat-

alysts, the NiAl<sub>7/4</sub> catalyst with the NiAl major phase showed the highest conversion. Combined with the phase-state analysis results obtained by XRD and TEM, it can be ascertained that the catalytic activity of NiAl is much higher than that of pure metallic Ni and that of the other Ni–Al IMCs (Ni<sub>3</sub>Al and Ni<sub>2</sub>Al<sub>3</sub>). The results can be well understood through a combination of site isolation and the alteration of the electronic structure by chemical bonding.<sup>[23,24]</sup> The selectivity of the products shows that naphthalene hydrogenation to tetralin is the main reaction (100% selectivity to tetralin at a contact time lower than 1.87 h). Decalin as a final product is only detected in a very small amount at a high contact time (3.11 h), and the main product is tetralin with a selectivity of 98% over the NiAl<sub>7/4</sub> catalyst, which indicates that the hydrogenation of tetralin is a rate-controlled step over the Ni–Al IMCs. This phenomenon is similar to naphthalene hydrogenation over carbides and silicides.<sup>[25,26]</sup> Product selectivity of the hydrogenation of naphthalene versus the contact time over the NiAl<sub>7/4</sub> catalyst (as shown in Figure S4) further confirms these semihydrogenation properties. Comparing the Ni–Al IMCs catalysts with conventional naphthalene hydrogenation catalysts, even though the activity of the Ni–Al IMCs was lower than that of NiO/SiO<sub>2</sub>-Al<sub>2</sub>O<sub>3</sub>,<sup>[3]</sup> the selectivity to tetralin and stability were greatly enhanced.

To correlate the different activities among the Ni–Al IMCs, the apparent rate constant of naphthalene hydrogenation was calculated. Assuming pseudo-first-order kinetics for the hydrogenation of naphthalene, the rate constant  $k_a$  [h<sup>-1</sup>] was calculated at a low conversion on the basis of the first-order-reaction rate equation [Eq. (2)]:

$$-\ln(1-x_a) = k_a t \quad (2)$$

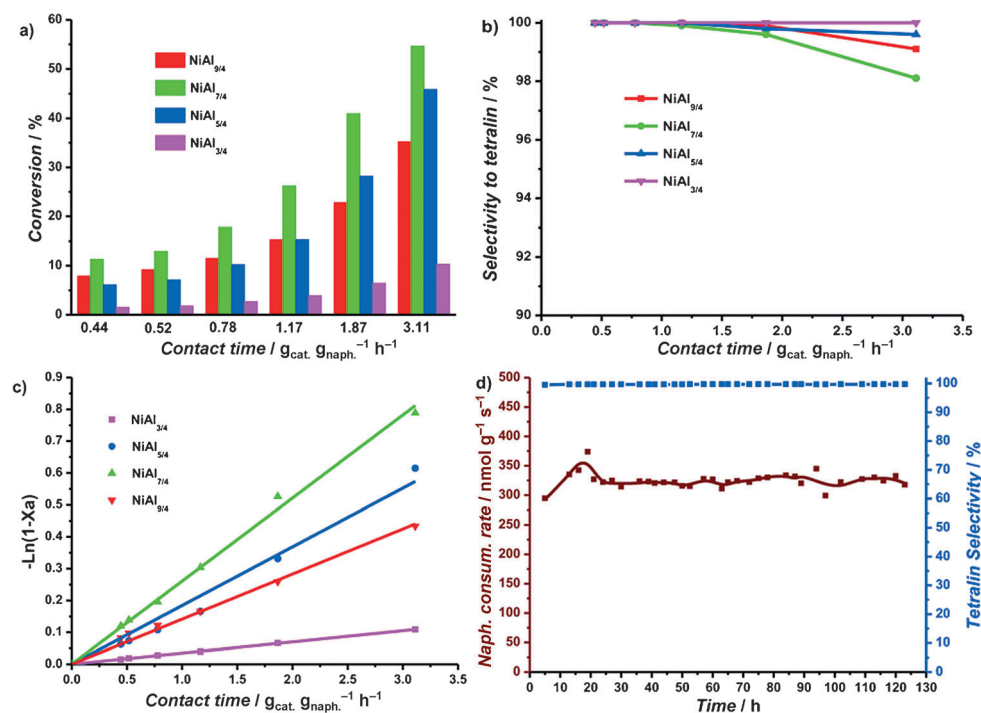


Figure 5. a) Conversion of naphthalene and b) selectivity to tetralin versus the contact time at 4.0 MPa H<sub>2</sub> and 340 °C over Ni–Al IMCs catalysts. c) Fitting of the pseudo-first-order kinetic model to the experimental data for the hydrogenation of naphthalene. d) Hydrogenation of naphthalene as a function of time on the NiAl<sub>7/4</sub> IMC catalyst.

in which  $x_a$  is the substrate consumption rate and  $t$  is the contact time.

As shown in Figure 5c, the substrate consumption rate  $[-\ln(1-x_a)]$  is linearly related to the contact time ( $t$ ), and consequently, naphthalene hydrogenation over Ni–Al IMCs catalysts is a pseudo-first-order reaction. The rate constant for the NiAl<sub>3/4</sub>, NiAl<sub>5/4</sub>, NiAl<sub>7/4</sub>, and NiAl<sub>9/4</sub> catalysts is 0.04, 0.18, 0.26, and 0.14 h<sup>-1</sup>, respectively (Table 2). This result further confirms that the catalytic activity of NiAl is superior to that of the Ni<sub>3</sub>Al

| Catalyst            | $K_a$ [h <sup>-1</sup> ] | Conversion [mol%] | Consumption rate of naphthalene [nmol g <sup>-1</sup> s <sup>-1</sup> ] | Selectivity [mol%] |
|---------------------|--------------------------|-------------------|---|--------------------|
| NiAl <sub>3/4</sub> | 0.04                     | 3.9               | 71.9  | 100                |
| NiAl <sub>5/4</sub> | 0.18                     | 15.3              | 283.2   | 100                |
| NiAl <sub>7/4</sub> | 0.26                     | 26.2              | 486.8   | 99.9               |
| NiAl <sub>9/4</sub> | 0.14                     | 15.3              | 284.0   | 100                |

and Ni<sub>2</sub>Al<sub>3</sub> IMCs and to that of metallic Ni. The naphthalene consumption rate also presents a similar relationship for the four catalysts in the hydrogenation of naphthalene. In addition, the selectivity to tetralin over the Ni–Al IMCs catalysts is almost close to 100%. Armbrüster et al. observed that the structural situations of Al<sub>13</sub>Fe<sub>4</sub> and Al<sub>13</sub>Co<sub>4</sub> resemble that of Ga-only coordinated Pd atoms in the GaPd IMC,<sup>[12, 13]</sup> which has been proven to be an excellent semihydrogenation catalyst. Therefore, the efficient and highly selective hydrogenation performance of Ni–Al IMCs can be attributed to the special geometry and electronic structure resulting from covalent interactions between the Ni and Al atoms.

To test the stability of the catalyst, the time course of naphthalene hydrogenation activity was observed for 125 h on the NiAl<sub>7/4</sub> IMC catalyst at 360 °C, under H<sub>2</sub> pressure of 4 MPa, with a contact time of 0.44 h. In Figure 5d, it is revealed that the naphthalene consumption rate was initially 295 nmol g<sup>-1</sup> s<sup>-1</sup> at 5 h and it then increased to 325 nmol g<sup>-1</sup> s<sup>-1</sup> at 20 h. Excitingly, NiAl<sub>7/4</sub> showed high stability and very high tetralin selectivity of 100% up to 125 h. A similar result was observed on Pd–Ga IMC catalysts used in alkyne-selective hydrogenation.<sup>[27]</sup> The effect of Ni–Al IMCs on the structure stability was determined from measurements of phase state and carbon content in the spent catalyst by using XRD and thermogravimetry, respectively, as shown in Figure 6. The XRD patterns show that the structure of NiAl is almost invariant after the stability test, whereas a new phase of Ni<sub>3</sub>Al appears with reference to the standard tetragonal-phase Ni<sub>3</sub>Al (JCPDS No. 09-0097); consequently, part of NiAl is reduced to Ni<sub>3</sub>Al under reaction conditions that, to some extent, follow the reaction  $3\text{NiAl} + 3\text{H}_2 \rightarrow \text{Ni}_3\text{Al} + 2\text{AlH}_3$ .<sup>[28]</sup> In addition, the thermogravimetry curve of the spent NiAl<sub>7/4</sub> IMC catalyst shows that only 5% of mass was lost from 60 to 110 °C, and this can be attributed to removal of surface physisorbed reaction substrates. However, there is no mass loss

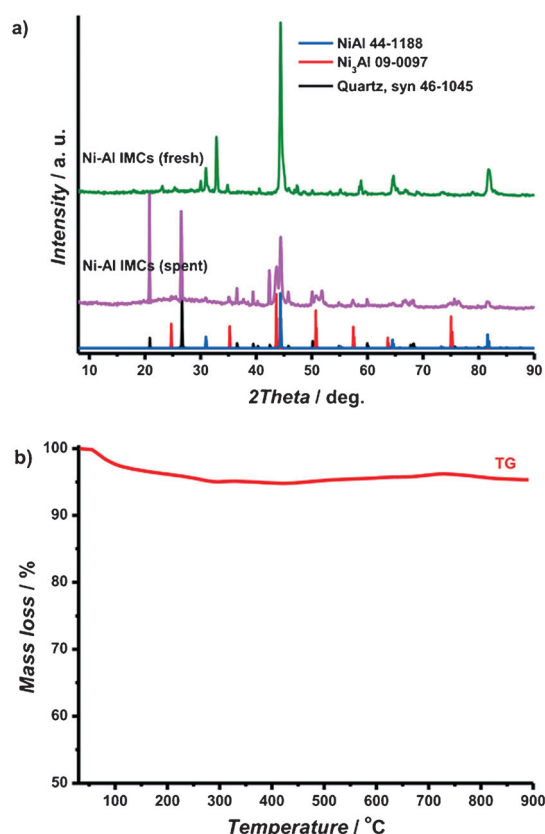


**Figure 6.** a) XRD patterns for the fresh and spent NiAl<sub>7/4</sub> IMC catalyst (after 125 h) in the hydrogenation of naphthalene. b) Thermogravimetry (TG) curve of the spent NiAl<sub>7/4</sub> IMC catalyst used to test carbon deposition.

peak in the high-temperature region (110–850 °C); consequently, carbon species are not formed on the catalysts during the hydrogenation of naphthalene. Ni atoms are scattered and spatially isolated by aluminum, which is similar to Ga-modified Pd-based IMC surfaces.<sup>[29,30]</sup> This in turn resists carbon deposition. The results show that Ni–Al IMCs are promising catalysts for semihydrogenation, which can be of high importance in fine-chemical synthesis industries.

## Conclusions

In summary, Ni–Al intermetallic compound catalysts with different phases were examined for the selective hydrogenation of naphthalene to tetralin. It was found that NiAl is a highly active and selective catalyst with long-term stability. The catalyst is highly resistant to coking and remains active for prolonged reaction times, which confirms that intermetallic compounds can be broadly applied in heterogeneous catalysis.

## Experimental Section

The Ni–Al IMCs were prepared by a chemical synthesis route. Typically, a mixture of anhydrous NiCl<sub>2</sub> (1.056 g, 8.15 mmol) and LiAlH<sub>4</sub> (0.541 g, 14.26 mmol) in 1,3,5-trimethylbenzene (30 mL) was heated at reflux at 164 °C for 12 h. The resulting gray-black precipi-

tate was collected after removing the solvent by centrifugation, and the solid was dried under high vacuum at 70 °C. To synthesize the nickel aluminide with various phases, the molar ratio of NiCl<sub>2</sub> and LiAlH<sub>4</sub> was controlled at 4:3, 4:5, 4:7, and 4:9. A 0.50 g portion of the as-precipitated black solid was loaded into a tubular furnace and calcined at 650 °C for 3 h under an atmosphere of Ar. The obtained solids were designated as NiAl<sub>3/4r</sub>, NiAl<sub>5/4r</sub>, NiAl<sub>7/4r</sub> and NiAl<sub>9/4r</sub> respectively.

X-ray diffraction (XRD) analysis was performed by using a Rigaku D/Max-RB diffractometer with a CuK<sub>α</sub> monochromated radiation source. Elemental analyses of the catalysts, including the metal Ni or Al, were detected by inductively coupled plasma atomic emission spectroscopy (ICP-AES). Nitrogen adsorption and desorption isotherms were measured by using an Autosorb IQ surface-area and pore-size analyzer. The morphology and structures of the as-prepared products were analyzed by using high-resolution field-emission scanning electron microscopy (FE-SEM, Nova NanoSEM 450 from FEI Company) and transmission electron microscopy (TEM, Tecnai G2 F30 S-Twin). Surface compositions were investigated by X-ray photoelectron spectroscopy (XPS) by employing an ESCALAB250 (Thermo VG, USA) spectrometer. Details are given in the Supporting Information.

The catalytic activities of the Ni–Al IMCs catalysts were tested for the hydrogenation of naphthalene at 340 °C at a H<sub>2</sub> pressure of 4.0 MPa, which was performed in a continuous fixed-bed reactor. The liquid reactant was composed of 1 wt% *n*-decane (as internal standard for GC analysis), 5 wt% naphthalene reactant, and varying amounts of *n*-octane (as solvent). Prior to the activity test, the passivated catalysts (0.20 g, diluted with quartz sand to 5 mL) were activated in situ with H<sub>2</sub> at 450 °C and 4 MPa for 4 h. The experimental data were collected at different contact times until the fresh catalyst reached a steady state for 12 h. Variation of the contact time was achieved by changing the flow rate of the liquid reactants from 0.03 to 0.21 mLmin<sup>-1</sup>. The contact time is defined in Equation (3):

$$\tau = \frac{W_{\text{cat}}}{n_{\text{feed}}} \quad (3)$$

in which  $W_{\text{cat}}$  denotes the catalyst weight and  $n_{\text{feed}}$  denotes the total molar flow fed to the reactor. Product identification was performed with an Agilent 6890 gas chromatograph equipped with a HP-5 MS capillary column and an Agilent 5973 mass-selective detector.

## Acknowledgements

We gratefully acknowledge financial support provided by the National Natural Science Foundation of China (21373038 and 21403026), the China Postdoctoral Science Foundation (2014M551068), and the Fundamental Research Funds for the Central Universities (DUT14RC(3)007). We thank Dr. Alex C. W. Tsang for improving the English in this paper.

**Keywords:** aluminum · hydrogenation · intermetallic compounds · nickel · wet chemistry

- [1] S. Hodoshima, H. Nagata, Y. Saito, *Appl. Catal. A* **2005**, *292*, 90–96.
- [2] Y. Cheng, H. Fan, S. Wu, Q. Wang, J. Guo, L. Gao, B. Zong, B. Han, *Green Chem.* **2009**, *11*, 1061–1065.
- [3] S. R. Kirumakki, B. G. Shpeizer, G. V. Sagar, K. V. R. Chary, A. Clearfield, *J. Catal.* **2006**, *242*, 319–331.
- [4] C. S. Song, X. L. Ma, *Appl. Catal. B* **2003**, *41*, 207–238.
- [5] B. H. Cooper, B. B. L. Donniss, *Appl. Catal. A* **1996**, *137*, 203–223.
- [6] C. S. Song, A. D. Schmitz, *Energy Fuels* **1997**, *11*, 656–661.
- [7] M. Crespo-Quesada, F. Cárdenas-Lizana, A. Dessimoz, L. Kiwi-Minsker, *ACS Catal.* **2012**, *2*, 1773–178.
- [8] S. X. McFadden, R. S. Mishra, R. Z. Valiev, A. P. Zhilyaev, A. K. Mukherjee, *Nature* **1999**, *398*, 684–686.
- [9] I. Baker, E. P. George in *The Encyclopedia of Materials: Science and Technology* (Eds.: K. H. J. Buschow, R. W. Cahn, M. C. Flemings, B. Ilshner, E. J. Kramer, S. Mahajan), Elsevier Press, Pergamon **2001**, pp. 4225–4232.
- [10] J. Zou, C. L. Fu, *Phys. Rev. B* **1995**, *51*, 2115–2121.
- [11] B. Ganem, J. O. Osby, *Chem. Rev.* **1986**, *86*, 763–780.
- [12] M. Armbrüster, K. Kovnir, M. Friedrich, D. Teschner, G. Wowsnick, M. Hahne, P. Gille, L. Szentmiklósi, M. Feuerbacher, M. Heggen, F. Girgsdies, D. Rosenthal, R. Schlögl, Y. Grin, *Nat. Mater.* **2012**, *11*, 690–693.
- [13] M. Armbrüster, R. Schlögl, Y. Grin, *Sci. Technol. Adv. Mater.* **2014**, *15*, 034803–034821.
- [14] L. Piccolo, *Chem. Commun.* **2013**, *49*, 9149–9151.
- [15] J. A. Haber, N. V. Gunda, J. J. Balbach, M. S. Conradi, W. E. Buhro, *Chem. Mater.* **2000**, *12*, 973–982.
- [16] D. P. Dutta, G. Sharma, A. K. Rajarajan, S. M. Yusuf, G. K. Dey, *Chem. Mater.* **2007**, *19*, 1221–1225.
- [17] J. A. Haber, J. L. Crane, W. E. Buhro, C. A. Frey, S. M. L. Sastry, J. J. Balbach, M. S. Conradi, *Adv. Mater.* **1996**, *8*, 163–166.
- [18] N. Ohtsu, M. Oku, T. Shishido, K. Wagatsuma, *Appl. Surf. Sci.* **2007**, *253*, 8713–8717.
- [19] F. U. Hillebrecht, J. C. Fuggle, P. A. Bennett, Z. Zolnieriek, Ch. Freiburg, *Phys. Rev. B* **1983**, *27*, 2179.
- [20] K. Kovnir, M. Armbrüster, D. Teschner, T. V. Venkov, F. C. Jentoft, A. Knop-Gericke, Y. Grin, R. Schlögl, *Sci. Technol. Adv. Mater.* **2007**, *8*, 420–427.
- [21] M. Armbrüster, K. Kovnir, M. Behrens, D. Teschner, Y. Grin, R. Schlögl, *J. Am. Chem. Soc.* **2010**, *132*, 14745–14747.
- [22] N. Ohtsu, A. Nomura, M. Oku, T. Shishido, K. Wagatsuma, *Appl. Surf. Sci.* **2008**, *254*, 5336–5341.
- [23] X. Chen, A. Q. Zhao, Z. F. Shao, C. Li, C. T. Williams, C. H. Liang, *J. Phys. Chem. C* **2010**, *114*, 16525–16533.
- [24] X. Chen, M. Li, J. C. Guan, X. K. Wang, C. T. Williams, C. H. Liang, *Ind. Eng. Chem. Res.* **2012**, *51*, 3604–3611.
- [25] M. Pang, C. Y. Liu, W. Xia, M. Muhler, C. H. Liang, *Green Chem.* **2012**, *14*, 1272–1276.
- [26] C. H. Liang, A. Q. Zhao, X. F. Zhang, Z. Q. Ma, R. Prins, *Chem. Commun.* **2009**, 2047–2049.
- [27] A. Ota, J. Kröhnert, G. Weinberg, I. Kasatkin, E. L. Kunkes, D. Ferri, F. Girgsdies, N. Hamilton, M. Armbrüster, R. Schlögl, M. Behrens, *ACS Catal.* **2014**, *4*, 2048–2059.
- [28] R. Moskovic, *J. Mater. Sci.* **1977**, *12*, 489–493.
- [29] J. Osswald, R. Giedigkeit, R. E. Jentoft, M. Armbrüster, F. Girgsdies, K. Kovnir, T. Ressler, Y. Grin, R. Schlögl, *J. Catal.* **2008**, *258*, 210–218.
- [30] J. Osswald, K. Kovnir, M. Armbrüster, R. Giedigkeit, R. E. Jentoft, U. Wild, Y. Grin, R. Schlögl, *J. Catal.* **2008**, *258*, 219–227.

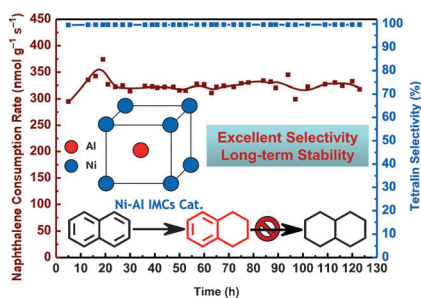
Received: November 28, 2014

Revised: January 4, 2015

Published online on ■■■■■, 0000

## FULL PAPERS

**Selecting the best:** Ni–Al intermetallic compounds (IMCs) are successfully prepared by a chemical synthesis route. These compounds present good activity, high selectivity, and long-term stability in the semihydrogenation of naphthalene to tetralin owing to alteration of the electronic structure by chemical bonding.



X. Chen, Y. Ma, L. Wang, Z. Yang, S. Jin,  
L. Zhang, C. Liang\*



**Nickel–Aluminum Intermetallic  
Compounds as Highly Selective and  
Stable Catalysts for the  
Hydrogenation of Naphthalene to  
Tetralin**

